nanomaterials

MDPI

Article

Oscillations of As Concentration and Electron-to-Hole Ratio in Si-Doped GaAs Nanowires

Vladimir G. Dubrovskii [1,*] and Hadi Hijazi [2]

[1] Universitetskaya Embankment. 13B, Saint Petersburg State University, 199034 Saint Petersburg, Russia
[2] Kronverkskiy prospekt 49, ITMO University, 197101 Saint Petersburg, Russia; hijazi@itmo.ru
* Correspondence: dubrovskii@mail.ioffe.ru

Received: 2 April 2020; Accepted: 22 April 2020; Published: 27 April 2020

Abstract: III–V nanowires grown by the vapor–liquid–solid method often show self-regulated oscillations of group V concentration in a catalyst droplet over the monolayer growth cycle. We investigate theoretically how this effect influences the electron-to-hole ratio in Si-doped GaAs nanowires. Several factors influencing the As depletion in the vapor–liquid–solid nanowire growth are considered, including the time-scale separation between the steps of island growth and refill, the "stopping effect" at very low As concentrations, and the maximum As concentration at nucleation and desorption. It is shown that the As depletion effect is stronger for slower nanowire elongation rates and faster for island growth relative to refill. Larger concentration oscillations suppress the electron-to-hole ratio and substantially enhance the tendency for the p-type Si doping of GaAs nanowires, which is a typical picture in molecular beam epitaxy. The oscillations become weaker and may finally disappear in vapor deposition techniques such as hydride vapor phase epitaxy, where the n-type Si doping of GaAs nanowires is more easily achievable.

Keywords: vapor–liquid–solid growth; GaAs nanowires; Si doping; electron-to-hole ratio; oscillations of as concentration

1. Introduction

Semiconductor nanowires (NWs) show great promise as fundamental building blocks for use in nanoscience and nanotechnology [1–3]. III–V NWs and heterostructures based on such NWs are interesting for applications in nanophotonic devices, particularly those monolithically integrated with a Si electronic platform [4–10]. These applications of III–V NWs require a controllable methodology for their n-type and p-type doping. Consequently, significant efforts have been put into the investigation of the NW doping process (see, for example, references [11–13] for a review). Most III–V NW are epitaxially grown by the vapor–liquid–solid (VLS) method with metal droplets [14]. Si is routinely used as an n-type dopant of planar GaAs layers in molecular beam epitaxy (MBE) [15], but it often becomes a p-type dopant for VLS GaAs NWs [16–22]. This amphoteric effect has been attributed to a low As concentration in metal droplets, catalyzing the VLS growth of GaAs NWs [22].

Due to a low As content in a catalyst droplet, a fractional monolayer (ML) of GaAs NW rapidly consumes a substantial fraction of as atoms available for growth, after which the droplet must be refilled from vapor. This leads to the so-called nucleation antibunching in NWs [23] and manifests in the periodically changing morphology of the growth interface, which is detectable by the in situ growth monitoring of GaAs NWs inside a transmission electron microscope (TEM) [24–27]. For very low As content, fractional ML can even stop growing at a certain size and then evolve much slower at a rate of refill [28]. Periodic oscillations of the As concentration over the ML growth cycle further decrease the average electron-to-hole ratio achievable with Si doping of VLS GaAs NWs and therefore increase the tendency for p-type doping. This effect has recently been studied in Reference [29]

under the assumption of instantaneous ML growth until reaching the "stopping" size. Instantaneous development of the ML in the initial stage requires that the characteristic time of island growth τ is much shorter than the equivalent deposition time of 1 ML t_{ML}, which is inversely proportional to the As deposition rate. Such a time-scale separation is long known in the NW growth modeling [30] and is confirmed by in situ growth monitoring in a TEM [24–27].

However, we note that in situ TEM data are obtained for relatively low NW growth rates, typically less than 0.15 ML/s, which is usual for molecular beam epitaxy (MBE). The growth rates can be much faster in vapor phase deposition techniques, reaching approximately 15 ML/s in the extreme case of Au-catalyzed GaAs NWs in hydride vapor phase epitaxy (HVPE) [31]. Such a huge difference (approximately 100 times) does not guarantee that the strong inequality $\tau/t_{ML} \ll 1$ is satisfied in the entire range of possible VLS growth conditions (separation of the ML nucleation, growth, and refill has recently been investigated in Reference [32] from a different perspective). Here, we investigate theoretically self-regulated oscillations of group V concentration in a catalyst droplet during the VLS growth of III–V NWs and their impact on the Si doping of GaAs NWs in the general case without the time-scale separation of the ML growth and refill. Our considerations should apply equally well to any epitaxy technique, which is not necessarily restricted to slow NW elongation. Several other factors influencing the As depletion are studied, including the "stopping effect" at very low As concentrations, the role of the maximum As concentration at nucleation, and its desorption at elevated growth temperatures. We map out the electron-to-hole ratio in Si-doped GaAs NWs in different regimes with either large concentration oscillations leading to the suppression of n-type doping, or very weak oscillations leading to negligible effect. These results should be useful for better understanding the concentration oscillations under different conditions and controlling the related Si doping process in VLS GaAs NWs.

2. Model

According to Reference [22], the ratio z of the atom fractions of silicon atoms replacing Ga and As atoms in solid GaAs is given by $z = \exp(\mu_5 - \mu_3 + A)$, with μ_5 and μ_3 as the chemical potentials of As (labeled "5") and Ga (labeled "3") atoms in a catalyst droplet (in thermal units of $k_B T$, with k_B as the Boltzmann constant and T as the absolute temperature), and A as a constant which represents the difference of internal energies of a GaAs cell with Si impurity replacing either the As or Ga atom. Replacing Ga with Si atoms creates an As−Si pair and produces electrons, whereas replacing As with Si atoms creates Ga−Si pairs and produces holes. Hence, $z = n/p$ is the ratio of electron-to-hole concentrations (electron-to-hole ratio for brevity). The NW is n-doped at $z > 1$ and p-doped at $z < 1$. The replaced atoms should be put back to liquid, which explains the presence of the corresponding chemical potentials in the equation. The tendency for n-type doping at larger $\mu_5 - \mu_3$ is clearly seen. This observation was used in Reference [22] to explain why adding the Si impurity to VLS GaAs NWs leads to predominantly p-type conductivity in MBE (low μ_5) [16–21] but yields n-type conductivity in HVPE (high μ_5) [22].

As discussed in detail in Reference [29], the main contribution to μ_5 is logarithmic [3,32,33], and it can be put as $\mu_5 = \ln\left(\theta_L/\theta_{eq}\right)$. Here, we present the As concentration in a catalyst droplet in terms of the effective coverage equivalent to the arsenic content in liquid, denoted θ_L, by normalizing the total number of As atoms in liquid to the number of As atoms (or GaAs pairs) in the full ML of a GaAs NW. In this normalization, the size of fractional ML θ changes from zero to unity, so θ represents the ML coverage. The equilibrium As content under no-growth conditions equals θ_{eq}, and it depends on the Ga concentration for Au-catalyzed VLS growth [33]. The As concentration in a catalyst droplet is always much lower than that of Ga [32]; therefore, the chemical potential oscillations over the ML formation cycle are due to oscillations of μ_5 at $\mu_3 \cong const$ [23]. For the Si doping of GaAs NWs, these considerations yield

$$\frac{z}{z_0} = \frac{\theta_L}{\theta_0}, \tag{1}$$

with z_0 as the maximum electron-to-hole ratio corresponding to the maximum As content at nucleation θ_0. The value of θ_0 is directly related to the nucleation-mediated NW growth rate for both Ga-catalyzed [34] and Au-catalyzed [35] VLS growths of GaAs NWs. This normalized electron-to-hole ratio oscillates in synchronization with the ML growth cycle. The average electron-to-hole ratio in the whole NW is obtained by the corresponding averaging of Equation (1) over one ML growth cycle.

The kinetics of the ML coverage and as concentration in liquid is described by [29]

$$\frac{d\theta}{dx} = \frac{\theta_L - \theta_{eq}}{\varepsilon},\ \frac{d\theta_L}{dx} + \frac{d\theta}{dx} = 1 - \left(\frac{\theta_L}{\theta_v}\right)^2. \quad (2)$$

The initial conditions are given by $\theta(t = 0) = 0$ and $\theta_L(t = 0) = \theta_0$. The parameters are defined as

$$x = t/t_{ML},\ \varepsilon = \tau/t_{ML}. \quad (3)$$

Clearly, x is the coverage equivalent to refill, which is proportional to the growth time t, and ε is the ratio of the island growth time τ over the deposition time t_{ML}. As discussed above, the previous results of Reference [29] correspond to the limiting case of instantaneous growth at $\varepsilon \to 0$. Equation (2) for θ shows that the fractional ML progresses at the rate ε in this normalization when $\theta_L > \theta_{eq}$, and it stops growing when $\theta_L = \theta_{eq}$. Equation (2) for θ_L shows that the total number of As atoms in liquid and solid changes with time due to As deposition and desorption at the rate of refill. Quadratic dependence of the desorption term on θ_L is due to the desorption of As in the form of As_2 molecules [33]. The desorption rate from the droplet is determined by the equivalent as content θ_v corresponding to equilibrium of this droplet with vapor providing a given flux onto the droplet surface. The average electron-to-hole ratio is given by

$$\frac{\langle z \rangle}{z_0} = \frac{1}{\theta_0\left(x_g + x_r\right)} \int_0^{x_g + x_r} dx \theta_L(x). \quad (4)$$

Here, x_g and x_r are the normalized growth times of the ML growth and the refill stages, respectively, which are defined as

$$\theta\left(x_g\right) = 1,\ \theta_L\left(x_g + x_r\right) = \theta_0. \quad (5)$$

Our model contains four plausible parameters: θ_0 standing for the initial as content at nucleation, θ_{eq} for its equilibrium content, θ_v for desorption, and ε for the growth kinetics. The parameters θ_0, θ_{eq}, and θ_v scale linearly with the corresponding atomic concentrations of As and with the NW radius R, so all θ are proportional to R at the fixed concentrations. θ_v is inversely proportional to the square root of the vapor flux and hence decreases for lower fluxes. Lower θ_v corresponds to higher fractions of re-evaporated As atoms. The ML deposition time t_{ML} alone does not enter the equations but can be used to express all the results in the real time scale when required.

Without As desorption (at $\theta_v \to \infty$), we simply have $x_g + x_r = 1$, because the sum of the ML growth and refill times must equal the time of ML deposition. Solutions to Equation (2) in this case are obtained in the form

$$\theta = \left(\theta_0 - \theta_{eq} - \varepsilon\right)\left(1 - e^{-x/\varepsilon}\right) + x \quad (6)$$

$$\theta_L = \theta_0 - \theta + x,\ 0 \le x \le x_g \text{ and } \theta_L = \theta_0 - 1 + x,\ x_g \le x \le 1. \quad (7)$$

The minimum As content at the end of the ML growth stage is given by $\theta_{min} = \theta_L\left(x_g\right) = \theta_0 - 1 + x_g$.

We now note that the value of ε is naturally restricted to the range $0 \le \varepsilon \le \theta_0 - \theta_{eq}$. According to Equation (6), the minimum $\varepsilon = 0$ describes the instantaneous growth of fractional ML to either 1 (at $\theta_0 - \theta_{eq} \ge 1$) or the stopping size $\theta_0 - \theta_{eq}$ (at $\theta_0 - \theta_{eq} < 1$) [29]. The maximum $\varepsilon = \theta_0 - \theta_{eq}$ describes the slowest possible growth of fractional ML at the rate of refill, $\theta = x$, proceeding at a

time-independent As content in liquid, $\theta_L = \theta_0$. Using Equation (6) at $\theta(x_g) = 1$, the ML growth time at any ε is obtained in the form

$$x_g = 1 - (\theta_0 - \theta_{eq} - \varepsilon) + \varepsilon W\left[\frac{(\theta_0 - \theta_{eq} - \varepsilon)}{\varepsilon} exp\left(\frac{(\theta_0 - \theta_{eq} - \varepsilon - 1}{\varepsilon}\right)\right]. \quad (8)$$

Here, $W(X)$ is the Lambert function such that $Wexp(W) = X$. Due to $W(0) = 0$, Equation (8) gives $x_g = 1$ at $\varepsilon = \theta_0 - \theta_{eq}$, meaning that $x_r = 0$. In this limiting case of slow island growth at the deposition rate, its growth time simply equals the ML deposition time, while the droplet at a constant content requires no refill from vapor. At $\varepsilon \to 0$, solutions to Equation (8) behave very differently depending on whether the stopping size is absent (at $\theta_0 - \theta_{eq} > 1$) or present (at $\theta_0 - \theta_{eq} < 1$). At $\theta_0 - \theta_{eq} > 1$, the main asymptote of the Lambert function is logarithmic, yielding $\varepsilon W\{exp[(\theta_0 - \theta_{eq} - \varepsilon - 1)/\varepsilon]\} \to \theta_0 - \theta_{eq} - \varepsilon - 1$ and hence $x_g = 0$. This solution corresponds to instantaneous ML growth without the stopping size. On the other hand, at $\theta_0 - \theta_{eq} < 1$, the Lambert function tends to zero at $\varepsilon \to 0$, giving $x_g = 1 - (\theta_0 - \theta_{eq})$. This solution describes the instantaneous growth of fractional ML from zero to the stopping size $\theta_0 - \theta_{eq}$, which is followed by a much slower growth at the rate of refill.

Averaging Equation (7) gives the average electron-to-hole ratio in Si-doped GaAs NWs in the form

$$\frac{\langle z \rangle}{z_0} = \frac{(\theta_{eq} + \varepsilon)}{\theta_0} x_g + \left(1 - \frac{\theta_{eq} + \varepsilon}{\theta_0}\right)\varepsilon\left(1 - e^{-x_g/\varepsilon}\right) + \left(1 - \frac{1}{\theta_0}\right)(1 - x_g) + \frac{1}{2\theta_0}\left(1 - x_g^2\right), \quad (9)$$

where x_g is given by Equation (8). In the absence of desorption, Si doping depends on the three parameters θ_0, θ_{eq} and ε.

With As desorption, solutions to Equation (2) write

$$\theta = 2\beta\theta_v ln\left[cosh\left(\frac{\alpha x}{\theta_v}\right) + Csinh\left(\frac{\alpha x}{\theta_v}\right)\right] - \frac{(\theta_{eq} + \beta\theta_v)x}{\varepsilon} \quad (10)$$

$$\theta_L = \alpha\theta_v \frac{C + tanh\left(\frac{\alpha x}{\theta_v}\right)}{1 + Ctanh\left(\frac{\alpha x}{\theta_v}\right)} - \beta\theta_v,\ 0 \le x \le x_g, \quad (11)$$

with $\beta = \theta_v/(2\varepsilon)$, $\alpha = \sqrt{1 + \theta_{eq}/\varepsilon + \beta^2}$, and $C = (\theta_0/\theta_v + \beta)/\alpha$. In this more complex case, the normalized growth time can only be obtained numerically from Equation (10) at $\theta(x_g) = 1$. Then, the minimum As content in liquid $\theta_{min} = \theta_L(x_g)$ is calculated from Equation (11). After the ML is completed, the solution to Equation (2) for θ_L at $d\theta/dx = 0$ yields the result of Reference [29]:

$$\theta_L = \theta_v tanh\left[\frac{x - x_g}{\theta_v} + atanh\left(\frac{\theta_{min}}{\theta_v}\right)\right],\ x_g \le x \le x_g + x_r. \quad (12)$$

The normalized refill time is easily obtained from this equation in the form

$$x_r = \theta_v\left[atanh\left(\frac{\theta_0}{\theta_v}\right) - atanh\left(\frac{\theta_{min}}{\theta_v}\right)\right]. \quad (13)$$

The ML formation cycles end at $x_T = x_r + x_g > 1$. After some calculations, the average normalized electron-to-hole ratio can be presented as

$$\frac{\langle z \rangle}{z_0} = \frac{1}{(x_g + x_r)} \frac{\theta_v^2}{\theta_0}\left\{\frac{(\alpha - \beta)x_g}{\theta_v} + ln\left[\frac{C + 1 - (C - 1)e^{-2\alpha x_g/\theta_v}}{2}\right] + ln\left[cosh\left(\frac{x_r}{\theta_v}\right) + \frac{\theta_{min}}{\theta_v} sinh\left(\frac{x_r}{\theta_v}\right)\right]\right\}, \quad (14)$$

and depends on the four parameters θ_0, θ_{eq}, θ_v, and ε.

3. Results and Discussion

Figure 1a shows the normalized ML growth time x_g as a function of ε in the absence of As desorption, where the refill time $x_r = 1 - x_g$. The curves were obtained from Equation (8) with different $\theta_0 - \theta_{eq}$ ranging from 0.35 to 2. In all cases, x_g monotonically increases with ε and reaches unity at $\varepsilon_{max} = \theta_0 - \theta_{eq}$, meaning that the ML growth takes a longer time for larger ε values. In the absence of the stopping effect (at $\theta_0 - \theta_{eq} > 1$), the curves start from zero at $\varepsilon = 0$, which corresponds to the instantaneous growth of the whole ML. In the presence of the stopping effect (at $\theta_0 - \theta_{eq} < 1$), a fractional ML evolves instantaneously only from zero to the stopping size $\theta_0 - \theta_{eq}$ and then grows at the rate of refill, which is why x_g is larger than zero at $\varepsilon = 0$ [29]. Figure 1b shows one cycle of the ML formation in terms of the ML coverage θ and As content in liquid θ_L versus the refill x. The curves were obtained from Equations (6) to (8) at a fixed $\theta_{eq} = 0.35$ and $\theta_0 = 0.7$, for two different values of ε. At a small $\varepsilon = 0.02$, there is a clear separation between the steps of fast growth of the ML coverage from zero to the stopping size of 0.35 ML and a much slower growth from 0.35 ML to the full ML. The As content rapidly drops to a value which is just slightly above equilibrium, and then it increases linearly to resume the initial value of 0.7 for the next nucleation event. At a large $\varepsilon = 0.3$, the ML grows almost at the rate of refill all the time, while the As content in liquid does not much change over the entire ML formation cycle. For the Si doping of GaAs NWs, the first case should yield a considerable drop of the electron-to hole ratio, while the second case should lead to an almost negligible effect due to the absence of concentration oscillations.

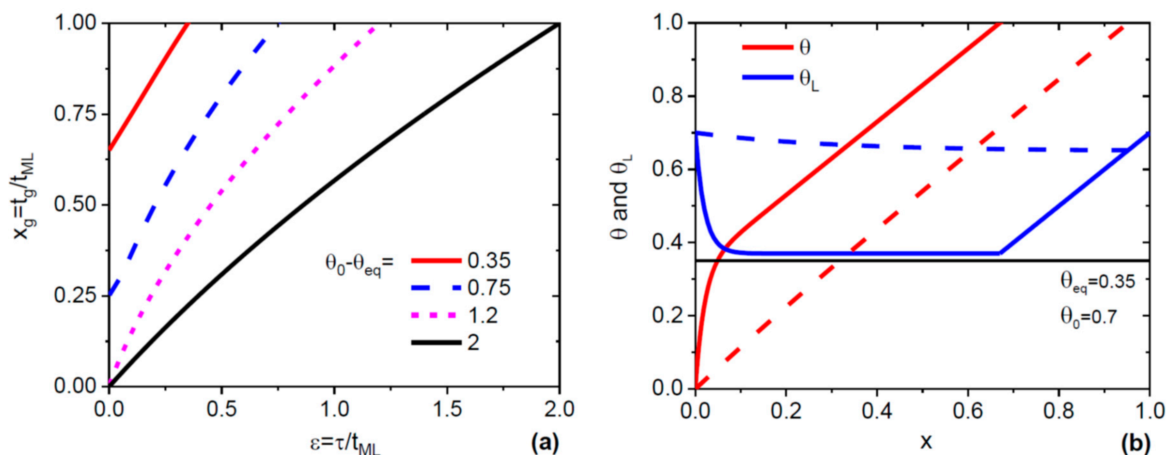

Figure 1. (**a**) Normalized monolayer (ML) growth time x_g as a function of ε for four different values of $\theta_0 - \theta_{eq}$ given in the legend, without As desorption. At the largest $\theta_0 - \theta_{eq} = 2$, x_g starts from zero and increases almost linearly with ε, reaching unity at ε_{max}. The curve at $\theta_0 - \theta_{eq} = 1.2$ is more non-linear but follows the same trend. Due to the stopping effect, x_g is nonzero at $\theta_0 - \theta_{eq} < 1$. (**b**) One oscillation of the ML coverage and As content in liquid at $\varepsilon = 0.02$ (solid lines) and $\varepsilon = 0.3$ (dashed lines). Different time scales of the fast and slow growth stages are clearly seen at $\varepsilon = 0.02$, where θ_L stays just slightly above equilibrium ($\theta_{eq} = 0.35$ is indicated by the horizontal line) for a long time. At $\varepsilon = 0.3$, the ML growth rate is very close to the rate of refill, while θ_L remains almost constant over the ML formation cycle.

Figure 2 shows the normalized electron-to-hole ratios in Si-doped GaAs as a function of ε and θ_0, along with the corresponding ML growth times, in the absence of as desorption. The curves in Figure 2a were obtained from Equations (8) and (9) at a fixed $\theta_0 = 0.7$ and two different $\theta_{eq} = 0.35$ and 0.05, where the stopping effect can be present. A smaller θ_{eq} yields stronger suppression of the electron-to-hole ratio due to larger oscillations of As concentration. In both cases, the curves of $\langle z \rangle / z_0$ are close to x_g, showing that the ML growth time is the main factor determining the electron-to-hole ratio. A smaller ε value always correspond to lower $\langle z \rangle / z_0$. Therefore, faster island growth rates relative to refill enhance the tendency for p-type Si doping of GaAs NWs. The curves in Figure 2b were obtained from Equations

(8) and (9) at a fixed $\varepsilon = 0.02$ (fast island growth relative to refill), and two different θ_{eq} = 0.35 for a higher and 0.05 for a lower growth temperature. The behavior of Si doping with θ_0 is non-monotonic in both cases, revealing the tendency for achieving a minimum electron-to-hole ratio at intermediate θ_0 . At low θ_0 close to equilibrium, the VLS growth proceeds under near-equilibrium conditions, where the Si doping should be almost the same as for planar layers. Very high θ_0 are equivalent to strongly non-equilibrium VLS growth without the stopping size, where the electron-to-hole ratio is less affected by the chemical potential oscillations.

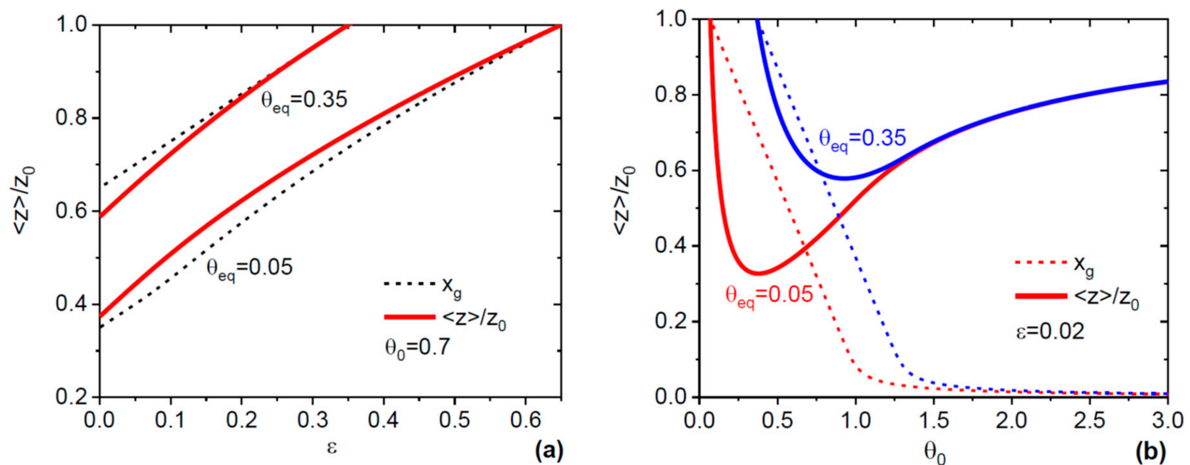

Figure 2. (**a**) Normalized electron-to-hole ratio in Si-doped GaAs nanowires (NWs) versus ε (solid lines) at a fixed $\theta_0 = 0.7$ and two different θ_{eq} = 0.35 and 0.05, corresponding to a higher and lower temperature, respectively. Short-dashed lines show the x_g values for the same parameters. The electron-to-hole ratio follows the same trend as the ML growth time, increasing quasi-linearly with ε from a minimum for instantaneous island growth to unity at $\varepsilon_{max} = \theta_0 - \theta_{eq}$. (**b**) Same as (**a**) but at a fixed $\varepsilon = 0.02$ as a function of θ_0. The values of $\langle z \rangle / z_0$ tend to unity when θ_0 is close to equilibrium (near-equilibrium growth conditions) and at large θ_0 (strongly non-equilibrium growth conditions), and they reach their minimum at intermediate θ_0.

Figure 3 illustrates how the ML growth kinetics influences the Si doping process in systems with as desorption. Figure 3a shows the ML coverage and as content in liquid versus refill. The curves were obtained from Equations (10) to (13) with $\theta_{eq} = 0.05$, $\theta_0 = 0.7$, and $\theta_v = 0.75$ (high desorption rates) for two different ε values. In the regime with fast island growth ($\varepsilon = 0.02$), the As content rapidly drops to a minimum, which is noticeably above equilibrium. The evolution of the system in the ML growth stage is indistinguishable of that without desorption, meaning that all the arriving As atoms are consumed by the growing ML and do not re-evaporate. After the ML is completed, the refill is strongly non-linear and takes a much longer time than without desorption, so the ML formation cycle ends at $x_T \cong 1.5$. The situation is very different at a large $\varepsilon = 0.5$, corresponding to slow island growth relative to refill. In this case, desorption becomes important already in the stage of ML growth. This stage is much longer than without desorption, with the As concentration decreasing more slowly to a minimum that is far above the equilibrium level. On the other hand, this minimum is lower than it would be without desorption. The refill is non-linear but faster than at a small $\varepsilon = 0.02$. Overall, the ML formation cycle is longer ($x_T \cong 1.9$) than in the previous case, which is mainly due to a longer ML growth stage.

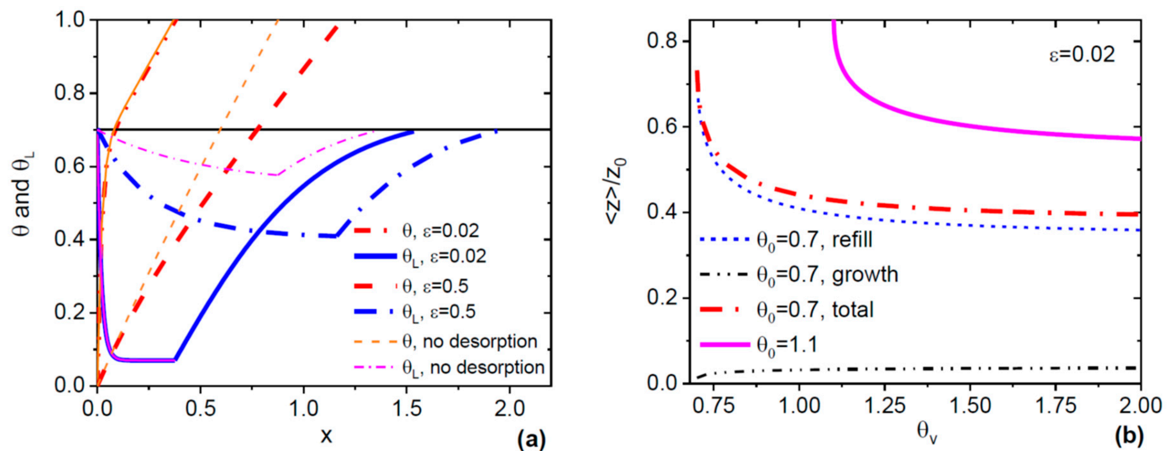

Figure 3. (**a**) One oscillation of the monolayer (ML) coverage and As content in liquid affected by As desorption, at $\theta_{eq} = 0.05$, $\theta_0 = 0.7$, $\theta_v = 0.75$, and two different $\varepsilon = 0.02$ (bold solid lines) and 0.5 (bold dashed lines). Thin lines show the corresponding behavior which would be observed without As desorption in the ML growth stage. At small ε, the growth stage is not affected by desorption, while the refill stage is prolongated. The As content drops very sharply as the ML grows. At large ε, the ML growth stage is much longer than without desorption and contributes to the total prolongation of the ML formation cycle. The As concentration varies much less than at small ε, as we saw earlier in Figure 1b. (**b**) Normalized electron-to-hole ratio in Si-doped GaAs NWs in systems with As desorption at a fixed $\varepsilon = 0.02$ versus θ_v, at two different $\theta_0 = 0.7$ and 1.1 (bold lines). At $\theta_0 = 0.7$, the dash-dotted and short-dashed lines show the contributions of the ML growth and refill stages into the resulting ratio $\langle z \rangle / z_0$. The contribution of refill is dominant for these parameters. At $\theta_0 = 1.1$, the ML growth is instantaneous, and the decrease of the electron-to-hole ratio is only due to refill. Overall, a smaller θ_0 yields a stronger suppression of n-type Si doping. The ratio $\langle z \rangle / z_0$ monotonically decreases with increasing θ_v, meaning that higher As desorption rates lead to larger electron-to-hole ratios.

Figure 3b shows the normalized electron-to-hole ratios in Si-doped GaAs in systems with desorption as a function of θ_v. The curves were obtained from Equations (10) to (13) at a fixed $\varepsilon = 0.02$ and $\theta_{eq} = 0.05$, with (at $\theta_0 = 0.7$) and without (at $\theta_0 = 1.1$) the stopping effect. The electron-to-hole ratio gradually decreases with increasing θ_v in both cases, showing that n-type Si doping is more suppressed for lower desorption rates. Deconvolution of the total ratio $\langle z \rangle / z_0$ in the regime with the stopping effect shows that the contribution of the refill stage dominates over the one due to ML growth.

Let us now formulate the most important trends for the concentration oscillations and the related Si doping of GaAs NWs in terms of temperature, NW growth rate, NW radius, and epitaxy technique. First, we have seen that larger oscillations of As concentration always lead to lower electron-to-hole ratios. The stopping effect always increases the amplitude of these oscillations, because the As concentration stays near equilibrium for a considerable fraction of the ML growth cycle. The stopping effect is observed at $\theta_0 - \theta_{eq} < 1$ and $\varepsilon \ll 1$, which requires (1) small NW radii, (2) slow NW growth rates (low θ_0), and (3) low growth temperatures to avoid desorption (high θ_v). Such growth regimes are more usual for the highly non-equilibrium MBE technique, where the Si doping leads to p-type conductivity [14–20]. Second, in the absence of the time-scale separation for the island growth and refill (large ε), we observe a new regime in which the ML develops at the rate of deposition without changing the As concentration in the droplet, and no refill is required. We suspect that such regimes occur in HVPE, which is a near-equilibrium growth process characterized by high temperatures and huge material inputs [31]. Metal organic vapor phase epitaxy (MOVPE) [32] is closer to equilibrium than MBE but yields lower NW growth rates compared to HVPE. Hence, an intermediate amplitude of the concentration oscillations is expected in MOVPE. This observation further supports the result of Ref. [22] for the n-type Si doping of HVPE-grown GaAs NWs. We strongly believe that a near-equilibrium VLS process should yield the Si doping levels in NWs similar with those in planar layers, as suggested

by the curves in Figures 2b and 3b. Third, the stopping effect is observed in situ only for wurtzite GaAs NWs with planar growth interface [26,27] (and growing at low rates). Zincblende NWs have the truncation at the top [24–27], which provides an additional source of material to complete the ML. This explains why the ML progression is instantaneous in truncated NWs. However, a truncated growth interface should not much affect the Si-doping process. When ML is rapidly completed by using a required amount of material from the truncation, the same amount of material must be returned to the truncation from vapor through the droplet. For Si doping, this process is equivalent to the continuing fractional ML above the stopping size at the equilibrium as concentration. Fourth, increasing θ_0 far above the equilibrium value always suppress the concentration oscillations and hence favors n-type Si doping, as seen in Figures 2b and 3b for small $\varepsilon \ll 1$. High θ_0 and low θ_{eq} correspond to MBE growth at low temperatures and high deposition rates (which also suppresses As desorption), so the n-type Si doping of MBE grown GaAs NWs is more probable in such regimes. Finally, here, we discussed only the VLS-type Si doping through the droplets. In many cases, Si [20] and other dopants [36,37] prefer to incorporate to NWs through their side facets or even the corners separating the facets in the vapor–solid (VS) mode. For the Si doping of GaAs NWs, the VS process should lead to n-type doping and compete with p-type doping by the VLS mechanism. A competition of the VLS versus VS Si doping occurs when the NW core is grown by the VLS mode through the droplet, and the shell is grown by a step-mediated VS process on the NW sidewalls. In this case, the shell should be n-doped, while the core should be p-doped. The VS incorporation in MBE is generally preferred to the VLS one at low temperatures [3], which should again favor n-type Si doping.

4. Conclusions

In conclusion, we have presented a fully analytic model for self-regulated oscillations of As concentration and the related electron-to-hole ratio in Si-doped GaAs NWs, which should be applicable in a wide range of epitaxy techniques. It has been shown that the oscillations and the Si doping process are generally controlled by the four parameters related to the maximum As concentration at nucleation, its equilibrium concentration, desorption, and the ratio of the island growth time over the deposition time. The influence of the latter parameter has never been studied before to our knowledge. However, it can completely suppress the oscillations in epitaxy techniques with very rapid NW growth rates. Generally, our study reveals the two limiting regimes of NW growth, with a large amplitude of concentration oscillations at slow NW growth rates, small NW radii, low As contents (often yielding the stopping effect), and near-equilibrium VLS processes with the slow progression of ML at an almost constant As concentration. The electron-to-hole ratio in Si-doped GaAs NWs is strongly suppressed in the first case, while in the second case, it remains the same as for the maximum as concentration at nucleation. Overall, these results should be useful for understanding and controlling the oscillatory behavior of As or P concentration in the VLS growth and the doping process in III–V NWs at low group V concentrations in the catalyst droplets.

Author Contributions: V.G.D. developed the model and H.H. did the simulations. All authors have read and agreed to the published version of the manuscript.

Funding: This research activity was supported by the Russian Science Foundation under the Grant 19-72-30004.

Acknowledgments: The authors gratefully acknowledge F. Glas for fruitful discussions.

Conflicts of Interest: The authors declare no conflict of interest.

References

1. Zhang, A.; Zheng, G.; Lieber, C.M. *Nanowires: Building Blocks for Nanoscience and Nanotechnology*; Springer: Berlin/Heidelberg, Germany, 2016.
2. Yang, P.; Yan, P.; Fardy, M. Semiconductor nanowires: what's next? *Nano Lett.* **2010**, *10*, 1529–1536. [CrossRef] [PubMed]

3. Dubrovskii, V.G. Theory of VLS Growth of Compound Semiconductors. In *Semiconductors and Semimetals*; Fontcuberta i Morral, A., Dayeh, S.A., Jagadish, C., Eds.; Academic Press: Cambridge, MA, USA, 2015; Volume 93, pp. 1–78.
4. Svensson, C.P.T.; Mårtensson, T.; Trägårdh, J.; Larsson, C.; Rask, M.; Hessman, D.; Samuelson, L.; Ohlsson, J. Monolithic GaAs/InGaP nanowire light emitting diodes on silicon. *Nanotechnology* **2008**, *19*, 305201. [CrossRef] [PubMed]
5. Dimakis, E.; Jahn, U.; Ramsteiner, M.; Tahraoui, A.; Grandal, J.; Kong, X.; Marquardt, O.; Trampert, A.; Riechert, H.; Geelhaar, L. Coaxial multishell (In, Ga)As/GaAs nanowires for near-infrared emission on Si substrates. *Nano Lett.* **2014**, *14*, 2604–2609. [CrossRef] [PubMed]
6. Thompson, M.D.; Alhodaib, A.; Craig, A.P.; Robson, A.; Aziz, A.; Krier, A.; Svensson, J.; Wernersson, L.-E.; Sanchez, A.M.; Marshall, A.R.J. Low leakage-current InAsSb nanowire photodetectors on silicon. *Nano Lett.* **2016**, *16*, 182–187. [CrossRef] [PubMed]
7. Wallentin, J.; Anttu, N.; Asoli, D.; Huffman, M.; Aberg, I.; Magnusson, M.H.; Siefer, G.; Fuss-Kailuweit, P.; Dimroth, F.; Witzigmann, B.; et al. InP nanowire array solar cells achieving 13.8% efficiency by exceeding the ray optics limit. *Science* **2013**, *339*, 1057–1060. [CrossRef] [PubMed]
8. Cirlin, G.E.; Bouravleuv, A.D.; Soshnikov, I.P.; Samsonenko, Y.B.; Dubrovskii, V.G.; Arakcheeva, E.M.; Tanklevskaya, E.M.; Werner, P. Photovoltaic properties of p-doped GaAs nanowire arrays grown on n-type GaAs(111)B substrate. *Nanoscale Res. Lett.* **2010**, *5*, 360–363. [CrossRef]
9. Karimi, M.; Jain, V.; Heurlin, M.; Nowzari, A.; Hussain, L.; Lindgren, D.; Stehr, J.E.; Buyanova, I.A.; Gustafsson, A.; Samuelson, L.; et al. Room-temperature InP/InAsP quantum discs-in-nanowire infrared photodetectors. *Nano Lett.* **2017**, *17*, 3356–3362. [CrossRef]
10. Stehr, J.E.; Dobrovolsky, A.; Sukrittanon, S.; Kuang, Y.; Tu, C.W.; Chen, W.M.; Buyanova, I.A. Optimizing GaNP coaxial nanowires for efficient light emission by controlling formation of surface and interfacial defects. *Nano Lett.* **2015**, *15*, 242–247. [CrossRef]
11. Dayeh, S.A.; Chen, R.; Ro, Y.G.; Sim, J. Progress in doping semiconductor nanowires during growth. *Mater. Sci. Semicond. Process.* **2017**, *62*, 135–155. [CrossRef]
12. Orrù, M.; Repiso, E.; Carapezzi, S.; Henning, A.; Roddaro, S.; Franciosi, A.; Rosenwaks, Y.; Cavallini, A.; Martelli, F.; Rubini, S. A roadmap for controlled and efficient n-type doping of self-assisted GaAs nanowires grown by molecular beam epitaxy. *Adv. Funct. Mater.* **2016**, *26*, 2836–2845. [CrossRef]
13. Goktas, N.I.; Fiordaliso, E.M.; LaPierre, R.R. Doping assessment in GaAs nanowires. *Nanotechnology* **2018**, *29*, 234001. [CrossRef] [PubMed]
14. Wagner, R.S.; Ellis, W.C. Vapor-liquid-solid mechanism of singe crystal growth. *Appl. Phys. Lett.* **1964**, *4*, 89. [CrossRef]
15. Schubert, E.F. *Doping in III-V Semiconductors*; Cambridge University Press: New York, NY, USA, 1993.
16. Piccin, M.; Bais, G.; Grillo, V.; Jabeen, F.; De Franceschi, S.; Carlino, E.; Lazzarino, M.; Romanato, F.; Businaro, L.; Rubini, S.; et al. Growth by molecular beam epitaxy and electrical characterization of GaAs nanowires. *Phys. E* **2007**, *37*, 134–137. [CrossRef]
17. Hilse, M.; Ramsteiner, M.; Breuer, S.; Geelhaar, L.; Riechert, H. Incorporation of the dopants Si and Be into GaAs nanowires. *Appl. Phys. Lett.* **2010**, *96*, 193104. [CrossRef]
18. Dimakis, E.; Ramsteiner, M.; Tahraoui, A.; Riechert, H.; Geelhaar, L. Shell-doping of GaAs nanowires with Si for n-type conductivity. *Nano Res.* **2012**, *5*, 796–804. [CrossRef]
19. Ketterer, B.; Mikheev, E.; Uccelli, E.; Fontcuberta i Morral, A. Compensation mechanism in silicon-doped gallium arsenide nanowires. *Appl. Phys. Lett.* **2010**, *97*, 223103. [CrossRef]
20. Dufouleur, J.; Colombo, C.; Garma, T.; Ketterer, B.; Uccelli, E.; Nicotra, M.; Fontcuberta i Morral, A. P-doping mechanisms in catalyst-free gallium arsenide nanowires. *Nano Lett.* **2010**, *10*, 1734–1740. [CrossRef]
21. Dementyev, P.A.; Dunaevskii, M.S.; Samsonenko, Y.B.; Cirlin, G.E.; Titkov, A.N. Current-voltage characteristics of silicon-doped GaAs nanowhiskers with a protecting AlGaAs coating overgrown with an undoped GaAs layer. *Semiconductors* **2010**, *44*, 610. [CrossRef]
22. Hijazi, H.; Monier, G.; Gil, E.; Trassoudaine, A.; Bougerol, C.; Leroux, C.; Castelluci, D.; Robert-Goumet, C.; Hoggan, P.; André, Y.; et al. Si doping of vapor-liquid-solid GaAs nanowires: N-type or p-type? *Nano Lett.* **2019**, *19*, 4498–4504. [CrossRef]
23. Glas, F.; Harmand, J.C.; Patriarche, G. Nucleation antibunching in catalyst-assisted nanowire growth. *Phys. Rev. Lett.* **2010**, *104*, 135501. [CrossRef]

24. Wen, C.-Y.; Tersoff, J.; Hillerich, K.; Reuter, M.C.; Park, J.H.; Kodambaka, S.; Stach, E.A.; Ross, F.M. Periodically changing morphology of the growth interface in Si, Ge, and GaP nanowires . *Phys. Rev. Lett.* **2011**, *107*, 025503. [CrossRef]
25. Jacobsson, D.; Panciera, F.; Tersoff, J.; Reuter, M.C.; Lehmann, S.; Hofmann, S.; Dick, K.A.; Ross, F.M. Interface dynamics and crystal phase switching in GaAs nanowires. *Nature* **2016**, *531*, 317. [CrossRef]
26. Harmand, J.C.; Patriarche, G.; Glas, F.; Panciera, F.; Florea, I.; Maurice, J.L.; Travers, L.; Ollivier, Y. Atomic step flow on a nanofacet. *Phys. Rev. Lett.* **2018**, *121*, 166101. [CrossRef]
27. Panciera, F.; Baraissov, Z.; Patriarche, G.; Dubrovskii, V.G.; Glas, F.; Travers, L.; Mirsaidov, U.; Harmand, J.C. Phase selection in self-catalyzed GaAs nanowires. *Nano Lett.* **2020**, *20*, 1669–1675. [CrossRef]
28. Dubrovskii, V.G. Refinement of nucleation theory for vapor-liquid-solid nanowires. *Cryst. Growth Des.* **2017**, *17*, 2589–2593. [CrossRef]
29. Dubrovskii, V.G.; Hijazi, H. Effect of arsenic depletion on the silicon doping of vapor-liquid-solid GaAs nanowires. *Phys. Stat. Sol. RRL* **2020**. [CrossRef]
30. Dubrovskii, V.G.; Sibirev, N.V.; Harmand, J.C.; Glas, F. Growth kinetics and crystal structure of semiconductor nanowires. *Phys. Rev. B* **2008**, *78*, 235301. [CrossRef]
31. Gil, E.; Dubrovskii, V.G.; Avit, G.; André, Y.; Leroux, C.; Lekhal, K.; Grecenkov, J.; Trassoudaine, A.; Castelluci, D.; Monier, G.; et al. Record pure zincblende phase in GaAs nanowires down to 5 nm in radius. *Nano Lett.* **2014**, *14*, 3938–3944. [CrossRef]
32. Maliakkal, C.B.; Mårtensson, E.K.; Tornberg, M.U.; Jacobsson, D.; Persson, A.R.; Johansson, J.; Wallenberg, R.L.; Dick, K.A. Independent control of nucleation and layer growth in nanowires. *ACS Nano* **2020**. [CrossRef]
33. Glas, F. Chemical potentials for Au-assisted vapor-liquid-solid growth of III-V nanowires. *J. Appl. Phys.* **2010**, *108*, 073506. [CrossRef]
34. Glas, F.; Ramdani, M.R.; Patriarche, G.; Harmand, J.C. Predictive modeling of self-catalyzed III-V nanowire growth. *Phys. Rev. B* **2013**, *88*, 195304. [CrossRef]
35. Dubrovskii, V.G.; Grecenkov, J. Zeldovich nucleation rate, self-consistency renormalization, and crystal phase of Au-catalyzed GaAs nanowires. *Cryst. Growth Des.* **2015**, *15*, 340–347. [CrossRef]
36. Chen, W.; Dubrovskii, V.G.; Liu, X.; Xu, T.; Larde, R.; Nys, J.P.; Grandidier, B.; Stievenard, D.; Patriarche, G.; Pareige, P. Boron distribution in the core of Si nanowire grown by chemical vapor deposition. *J. Appl. Phys.* **2012**, *111*, 094909. [CrossRef]
37. Dastjerdi, M.H.T.; Fiordaliso, E.M.; Leshchenko, E.D.; Akhtari-Zavareh, A.; Kasama, T.; Aagesen, M.; Dubrovskii, V.G.; LaPierre, R.R. Three-fold symmetric doping mechanism in GaAs nanowires. *Nano Lett.* **2017**, *17*, 5875–5882. [CrossRef]

© 2020 by the authors. Licensee MDPI, Basel, Switzerland. This article is an open access article distributed under the terms and conditions of the Creative Commons Attribution (CC BY) license (http://creativecommons.org/licenses/by/4.0/).